

Hilbert space fragmentation from lattice geometry

Pieter H. Harkema,* Michael Iversen,* and Anne E. B. Nielsen

Department of Physics and Astronomy, Aarhus University, DK-8000 Aarhus C, Denmark

The eigenstate thermalization hypothesis describes how isolated many-body quantum systems reach thermal equilibrium. However, quantum many-body scars and Hilbert space fragmentation violate this hypothesis and cause nonthermal behavior. We demonstrate that Hilbert space fragmentation may arise from lattice geometry in a spin-1/2 model that conserves the number of domain walls. We generalize a known, one-dimensional, scarred model to larger dimensions and show that this model displays Hilbert space fragmentation on the Vicsek fractal lattice of arbitrary generation. Using Monte Carlo methods, the model is characterized as strongly fragmented on the Vicsek fractal lattice when the number of domain walls is either small or close to the maximal value. We show that the model displays signatures similar to Hilbert space fragmentation on the second-generation hexaflake fractal lattice, the two-dimensional lattice, and a modified two-dimensional lattice. We study the autocorrelation function of local observables and demonstrate that the model displays nonthermal dynamics.

I. INTRODUCTION

Isolated, many-body, quantum systems are typically thermal, and the microcanonical ensemble accurately describes the expectation values of local observables at long times. The eigenstate thermalization hypothesis (ETH) explains this behavior from an ansatz about the matrix elements of local observables [1–3]. The ETH has been verified by numerous works (see Ref. [4] and references therein). However, several mechanisms violate the ETH and, as a consequence, cause nonthermal behavior.

Scarred models host a small number of ETH-violating energy eigenstates, called quantum many-body scars (QMBSs), embedded in an otherwise thermal spectrum [5–7]. While scar states are nonthermal, they only represent a weak violation of the ETH. QMBSs date back to the discovery of analytic excited energy eigenstates in the Affleck-Kennedy-Lieb-Tasaki model [8–10], and signatures of QMBSs were observed in experiments with kinetically constrained Rydberg atoms [11]. Since the initial findings, numerous scarred models have been discovered, e.g., Refs. [12–19], and QMBSs have been realized in various experimental setups [20–25].

Hilbert space fragmentation (HSF) represents another ETH-violating phenomenon where the Hilbert space is separated into dynamically disconnected subspaces even after resolving all symmetries [6]. These subspaces are called Krylov subspaces, and the number of subspaces grows exponentially with system size. The subspaces may vary in size from one-dimensional “frozen configurations” to subspaces with exponentially large dimensions. While the Krylov subspaces are not described by conventional quantum numbers associated with a symmetry of the Hamiltonian operator, they may be labeled by “statistically localized integrals of motion” [26] or commutant algebras [27]. HSF may represent a weak or strong violation of the ETH, and the corresponding

model is denoted as, respectively, weakly or strongly fragmented [28]. When the largest Krylov subspace constitutes a vanishingly small fraction of the relevant symmetry sector in the thermodynamic limit, the model is strongly fragmented. On the other hand, the model is weakly fragmented when the size of a Krylov subspace converges to the dimension of its symmetry sector in the thermodynamic limit. Although HSF violates the ETH, the Krylov subspaces may thermalize according to the Krylov-restricted ETH [29]. They may also be integrable or many-body localized [30, 31]. HSF has been extensively studied in models with charge and dipole conservation [28, 29, 32–34], but fragmentation also arises in other settings [35–44]. HSF is linked to Stark many-body localization where the effective Hamiltonian conserves both the charge and dipole moment [45, 46]. Consequently, signatures of HSF have been observed in experiments with the tilted Fermi-Hubbard model [47, 48].

The nature of fragmented models depends on the system dimension. For instance, the $t - J_z$ model displays HSF in one dimension [26], but it is not fragmented in two dimensions [27]. Likewise, while the pair-flip model displays HSF in one dimension, it is scarred in dimensions larger than one [27, 49]. Hence, the presence of HSF in one dimension does not guarantee its existence in higher dimensions. Several works have, however, constructed models that are HSF in dimensions larger than one [34, 50, 51]. These findings call for a better understanding of the connection between HSF and the number of spatial dimensions. Besides analyzing fragmentation in integer dimensions, a general analysis would naturally study HSF on finite generation fractal lattices. Fractal lattices have a more complicated structure, and one may wonder whether HSF can arise from the lattice geometry itself. If this is possible, then lattices may be constructed where HSF is present on certain sublattices but not on other sublattices.

In this work, we generalize a known, domain-wall conserving, one-dimensional, scarred model [17] to lattices of dimension larger than one. While the one-dimensional model hosts a few nonthermal scar states, the Hilbert

* These authors contributed equally to this work.

space shatters into numerous dynamically disconnected subspaces when the model is placed in higher dimensions. We study the model on the Vicsek fractal lattice, hexaflake fractal lattice, two-dimensional lattice, and a modified two-dimensional lattice. We show that the model displays HSF on the Vicsek fractal lattice of any generation and that the fragmentation is strong in symmetry sectors where the number of domain walls is either close to zero or close to the maximal number of domain walls. We observe features similar to HSF on all other considered lattices and we find that the level of fragmentation depends on the lattice geometry. This result is explained by lattice sites with more than two nearest neighbors confining the movement of domain walls. The combination of domain wall conservation and conservation of total magnetization was previously shown to cause HSF in a one-dimensional system [35], but we show that the domain wall conservation can be sufficient in higher dimensions. We demonstrate the nonthermal nature of the model by studying the time-averaged autocorrelation function of a local observable, and we compare the results with the Mazur bound.

In Sec. II, we take a one-dimensional, domain-wall conserving, scarred model as our starting point and generalize the model to larger dimensional lattices. We present the Vicsek fractal lattice, hexaflake fractal lattice, two-dimensional lattice, and a modified two-dimensional lattice. In Sec. III, we demonstrate that the model displays HSF on the Vicsek fractal lattice of arbitrary generation by explicitly constructing an exponential number of Krylov subspaces. Furthermore, we observe that the model displays characteristics similar to HSF on a section of the second-generation hexaflake fractal lattice, the two-dimensional lattice, and a modified two-dimensional lattice. We describe the mechanisms that restrict the movement of domain walls and cause fragmentation. For the Vicsek fractal lattice, we estimate the dimensions of symmetry sectors with a small number of domain walls using Monte Carlo importance sampling. We also estimate the dimension of the largest Krylov subspace in each symmetry sector. These results show that the largest Krylov subspace represents a vanishingly small part of the full symmetry sector. Hence, the model is strongly fragmented on the Vicsek fractal lattice for a small number of domain walls. We extend this result to symmetry sectors where the number of domain walls is close to the maximal value. In Sec. IV, we study the long-time average of the autocorrelation function of a local observable and compare the results with the Mazur bound. While the time-averaged autocorrelation function does not converge to the Mazur bound for the considered lattices, the Mazur bound becomes tight when the Hamiltonian is perturbed by a block diagonal random matrix. In Sec. V, we summarize the results.

II. MODEL

We take the model from Ref. [17] as our starting point. Consider a one-dimensional lattice of length N with open boundary conditions described by the Hamiltonian

$$H_{1D} = \lambda \sum_{i=2}^{N-1} (\sigma_i^x - \sigma_{i-1}^z \sigma_i^x \sigma_{i+1}^z) + \Delta \sum_{i=1}^N \sigma_i^z + J \sum_{i=1}^{N-1} \sigma_i^z \sigma_{i+1}^z, \quad (1)$$

where σ_i^x and σ_i^z are the Pauli x - and z -operators acting on site i . The kinetic term $\sigma_i^x - \sigma_{i-1}^z \sigma_i^x \sigma_{i+1}^z$ flips the spin on site i if the sum of the spins on the two nearest neighbors, sites $i-1$ and $i+1$, is zero. The second term in Eq. (1) represents an energy contribution ascribed to the spin orientation in a uniform magnetic field in the z -direction with strength Δ . The third term represents nearest neighbor interactions along the z -direction with strength J . When two nearest neighbor spins are in different states, the edge connecting the two sites is denoted as a domain wall. The Hamiltonian operator conserves the number of domain walls. This model has been shown to host two towers of QMBSs [17].

We generalize the one-dimensional model from Eq. (1) to higher dimensional lattices while preserving its characteristic features. In particular, the model should conserve the number of domain walls. We consider the Hamiltonian

$$H = H_\lambda + H_z + H_{zz} \quad (2)$$

with

$$H_\lambda = \lambda \sum_{\mathbf{r}} \delta \left(\sum_{\langle \mathbf{r}, \mathbf{r}' \rangle} \sigma_{\mathbf{r}'}^z \right) \sigma_{\mathbf{r}}^x, \quad (3a)$$

$$H_z = \Delta \sum_{\mathbf{r}} \sigma_{\mathbf{r}}^z, \quad (3b)$$

$$H_{zz} = J \sum_{\langle \mathbf{r}, \mathbf{r}' \rangle} \sigma_{\mathbf{r}}^z \sigma_{\mathbf{r}'}^z, \quad (3c)$$

where $\langle \cdot, \cdot \rangle$ refers to nearest neighbor sites, and δ is the function given by $\delta(0) = 1$ and $\delta(x) = 0$ for $x \neq 0$. The three-body kinetic terms in Eq. (1) are, hence, generalized to the operator H_λ consisting of many-body terms. The remaining terms in Eqs. (3b) and (3c) are similar to the one-dimensional model. We note that Eqs. (2) and (3) reduce to Eq. (1) for the one-dimensional lattice.

Equation (3a) implies that sites with an odd number of nearest neighbors display no dynamics. Therefore, we generally study lattices where all sites not on the lattice boundary have an even number of nearest neighbors. Furthermore, we introduce additional sites along the boundary such that boundary sites with an odd number of nearest neighbors get an even number of nearest neighbors. We hereby ensure that all sites in the original lattice are dynamically active. The newly added sites are inactive and we generally choose them as spin-down. We consider open boundary conditions for all lattices throughout this work. We study the Vicsek fractal

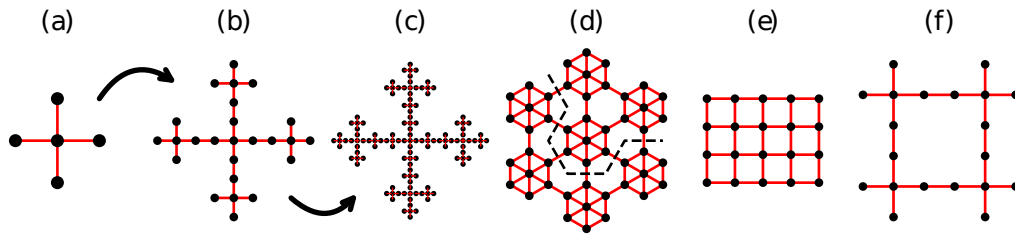


FIG. 1. Illustration of the considered lattices. Black dots show the lattice sites and red lines display nearest neighbor edges. (a) The first-generation Vicsek fractal lattice. (b) The second-generation Vicsek fractal lattice is obtained from generation one by substituting all lattice sites with five new sites. (c) Similarly, the third-generation Vicsek fractal lattice is obtained from generation two by substituting all sites with generation one Vicsek fractal lattices. (d) Second-generation hexaflake fractal lattice. We consider the lattice consisting of three connected first-generation hexaflake fractal lattices (above the dashed line). (e) Two-dimensional lattice of size 5×4 . (f) Modified two-dimensional lattice constructed from four connected first-generation Vicsek fractal lattices.

lattice, a section of the second-generation hexaflake fractal lattice, the two-dimensional lattice, and a modified two-dimensional lattice. Figure 1 displays the considered lattices. The figure also illustrates how the Vicsek fractal lattice of generation g is obtained from generation $g - 1$ by substituting all lattice sites with five new sites. All studied lattices have boundary sites with an odd number of nearest neighbors and thus get additional sites appended. Figure 2 illustrates the procedure of adding inactive sites along the boundary for the second-generation Vicsek fractal lattice.

III. HILBERT SPACE FRAGMENTATION

Fragmented models are characterized by the Hilbert space separating into kinetically disconnected subspaces

$$\mathcal{H} = \bigoplus_i \mathcal{K}_i, \quad (4a)$$

$$\mathcal{K}_i = \text{span}(\{H^n |\psi_i\rangle | n = 0, 1, 2, \dots\}), \quad (4b)$$

where \mathcal{H} is the full Hilbert space, \mathcal{K}_i denotes a Krylov subspace of dimension d_i , and $|\psi_i\rangle$ is a product state that generates \mathcal{K}_i .

We study the fragmentation of the model in Eq. (2) on different lattices by computing the size and number of Krylov subspaces. Let $|s_1 \dots s_N\rangle$ be a simultaneous eigenket of the Pauli matrices in the z -direction $\{\sigma_r^z\}$. We compute the Krylov subspace generated by a state $|s_1 \dots s_N\rangle$ by iterative look-up in the matrix representation of the kinetic part of the Hamiltonian H_λ . In essence, if $\langle s'_1 \dots s'_N | H_\lambda | s_1 \dots s_N \rangle \neq 0$ then $|s'_1 \dots s'_N\rangle$ resides to the same Krylov subspace as $|s_1 \dots s_N\rangle$. We utilize the conservation of the number of domain walls by considering each symmetry sector separately. For all considered lattices, we generally observe the Hilbert space separating into Krylov subspaces. However, the degree of fragmentation depends on the number of domain walls

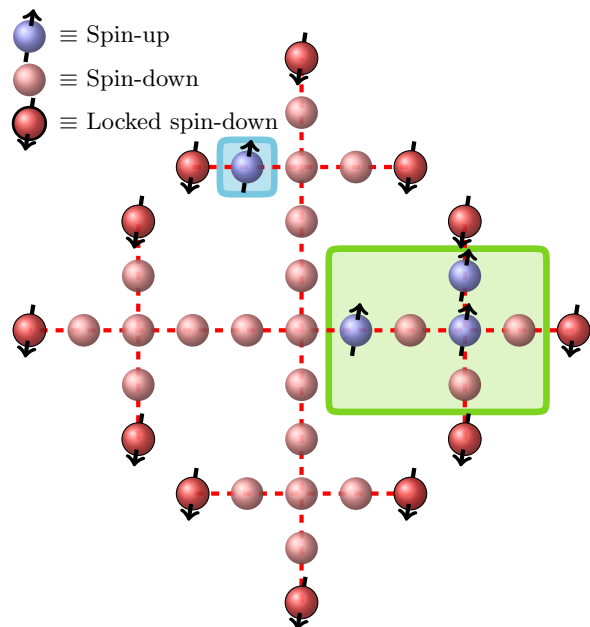


FIG. 2. The second-generation Vicsek fractal lattice padded with dynamically inactive sites along the boundary (dark red balls with black outlines and downward pointing arrows). The figure illustrates a product state in the symmetry sector with $n_{\text{dw}} = 8$ domain walls. Four sites are spin-up (blue balls with upward pointing arrows) and the remaining sites are spin-down (red balls). The sites inside the green box are denoted as an “active arm”. These sites may flip their spin and the domain walls may move around within the sublattice. Note, however, that the spin-down site connected to the active arm from the left (red ball at the center of the lattice) can not change its state to spin-up because three or more of its nearest neighbors are always spin-down. Therefore, this site effectively locks the dynamics within the active arm and all spin-down sites outside the green box can not be flipped. Similarly, the spin-up site inside the blue box is dynamically inactive and can not be flipped. Product states where all spins are dynamically inactive are denoted as “frozen states”, and we construct an exponential number of such states in Appendix B.

and the geometry of the lattice. Figure 3 displays the matrix representation of the Hamiltonian operator in the basis $\{|s_1 \dots s_N\rangle\}$ for each lattice. We show each symmetry sector separately, and the basis states are arranged to allow the block diagonal structure from Eq. (4). The gray pixels represent nonzero matrix elements while white pixels represent vanishing matrix elements.

A. Vicsek fractal lattice

The kinetic term in the Hamiltonian operator H_λ on the Vicsek fractal lattice is invariant under the transformation that inserts domain walls on edges where there is no domain wall and removes domain walls from edges where there is a domain wall. Therefore, the size and number of Krylov subspaces in the sector with n_{dw} domain walls are identical to size and number of the Krylov subspaces in the sector with $n_{\text{dw}}^{\text{max}} - n_{\text{dw}}$ domain walls, where $n_{\text{dw}}^{\text{max}}$ is the maximal number of domain walls on the Vicsek fractal lattice of generation g . Without loss of generality, we study sectors with less than or equal to half filling of domain walls, i.e., $n_{\text{dw}} \leq n_{\text{dw}}^{\text{max}}/2$. We further discuss this point in Appendix A.

Figure 3(a) displays the Hamiltonian operator for the second-generation Vicsek fractal lattice. We observe fragmentation within all symmetry sectors, with the amount of fragmentation varying between sectors. The fragmentation is caused by lattice sites with more than two nearest neighbors which may restrict the movement of domain walls. For instance, if all domain walls are located within one ‘‘arm’’ of the Vicsek fractal lattice, then the central spin can not be flipped, and it will act as a blockade for the movement of the domain walls as illustrated in Fig. 2. The dynamics of each Krylov subspace is, therefore, restricted to isolated regions on the lattice, with the remaining sites being frozen. In Appendix B, we formally demonstrate this point. We prove that the model displays HSF on the Vicsek fractal lattice of any generation by explicitly constructing an exponential number of one-dimensional Krylov subspaces.

Figure 3(a) illustrates that symmetry sectors with few domain walls seem to consist of many small Krylov subspaces. On the other hand, sectors with the number of domain walls close to $n_{\text{dw}}^{\text{max}}/2$ seem dominated by one large Krylov subspace. Hence, the Vicsek fractal lattice seems to display stronger fragmentation for fewer domain walls when $n_{\text{dw}} \leq n_{\text{dw}}^{\text{max}}/2$. We characterize the model as either weakly or strongly fragmented by studying the largest Krylov subspace in each symmetry sector. Let $\mathcal{H}_{n_{\text{dw}}}$ be the symmetry sector with n_{dw} domain walls, and let $D_{n_{\text{dw}}}$ be the dimension of this sector. Furthermore, let $d_{n_{\text{dw}}}^{\text{max}}$ be the dimension of the largest Krylov subspace in the sector with n_{dw} domain walls. The model is strongly fragmented if $\lim_{g \rightarrow \infty} (d_{n_{\text{dw}}}^{\text{max}}/D_{n_{\text{dw}}}) = 0$ and weakly fragmented if $\lim_{g \rightarrow \infty} (d_{n_{\text{dw}}}^{\text{max}}/D_{n_{\text{dw}}}) = 1$. However, an exact calculation of $D_{n_{\text{dw}}}$ and $d_{n_{\text{dw}}}^{\text{max}}$ is only feasible for small system sizes, i.e., for generations $g \leq 2$. For

larger generations, we utilize Monte Carlo importance sampling to estimate these quantities. We outline the numerical procedure in Appendix C. Figure 4 displays the ratio $d_{n_{\text{dw}}}^{\text{max}}/D_{n_{\text{dw}}}$ as a function of the lattice generation g for different symmetry sectors n_{dw} . The symmetry sector with no domain walls $n_{\text{dw}} = 0$ only consists of the state with all spins down $|\downarrow \downarrow \dots \downarrow\rangle$. Therefore, the ratio is unity for all generations. For all other considered sectors, the ratio $d_{n_{\text{dw}}}^{\text{max}}/D_{n_{\text{dw}}}$ decreases with increasing generation. These results indicate that the largest Krylov subspace represents a vanishing small part of the full symmetry sector. Therefore, the system displays strong fragmentation for sectors with a small number of domain walls.

The above analysis concerns symmetry sectors with less than or equal to half-filling of domain walls $n_{\text{dw}} \leq n_{\text{dw}}^{\text{max}}/2$. Recall that $d_{n_{\text{dw}}}^{\text{max}} = d_{n_{\text{dw}}'}^{\text{max}}$ and $D_{n_{\text{dw}}} = D_{n_{\text{dw}}'}$ with $n_{\text{dw}}' = n_{\text{dw}}^{\text{max}} - n_{\text{dw}}$. Therefore, the system also displays strong fragmentation in symmetry sectors where the number of domain walls is close to being maximal.

B. The hexaflake fractal lattice and two-dimensional lattice

Recall that sites with four or more nearest neighbors can restrict the movement of domain walls by acting as blockades. The second-generation hexaflake fractal lattice and the two-dimensional lattice are characterized by all sites having four or six nearest neighbors. Hence, we expect the model to display a large degree of fragmentation on these lattices since every site may act as a blockade. Figures 3(b) and 3(c) display the symmetry sectors of the Hamiltonian operator. As expected, the Hamiltonian operators on both lattices are split into numerous dynamically disconnected subspaces for a small number of domain walls similar to the result for the Vicsek fractal. However, for a large number of domain walls, the symmetry sectors display almost no fragmentation. We interpret this result as sites failing to act as blockades when the number of domain walls is large enough.

C. The modified two-dimensional lattice

The modified two-dimensional lattice is structurally similar to the Vicsek lattice as it is constructed from four first generation Vicsek fractals. It has both sites with four nearest neighbors, which may act as blockades, and sites with two nearest neighbors that do not restrict the movement of domain walls. However, in contrast to the Vicsek fractal, the modified two-dimensional lattice introduces a ‘‘loop’’. Figure 3(d) shows the Hamiltonian operator for each symmetry sector on the modified two-dimensional lattice. The loop reduces the amount of fragmentation in the modified two-dimensional lattice compared to the Vicsek fractal lattice. For $n_{\text{dw}} \geq 16$, no fragmentation is present. The presence of loops in the

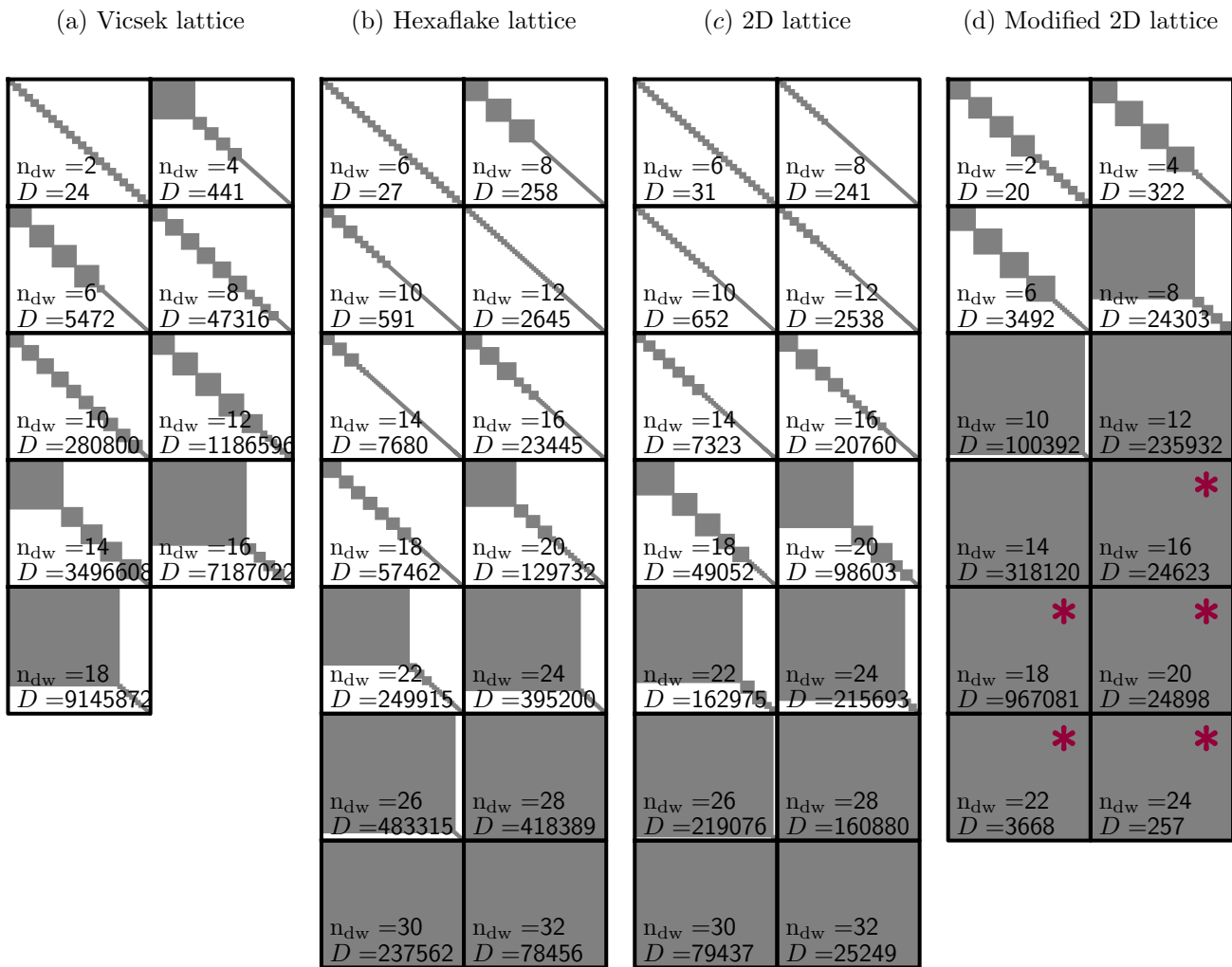


FIG. 3. Depictions of the Hamiltonian H for each symmetry sector. Gray pixels represent nonzero matrix elements and white pixels correspond to vanishing matrix elements. The figure illustrates the block diagonal structure of the Hamiltonian operator due to Hilbert space fragmentation. n_{dw} denotes the number of domain walls characterizing the symmetry sector, and $D \equiv D_{n_{dw}}$ denotes the dimension of the symmetry sector. The red asterisks mark symmetry sectors containing just a single Krylov subspace that spans the full sector. For the Vicsek fractal lattice, the Hamiltonian is only depicted up to $n_{dw} = 18$ domain walls since the Krylov subspaces in the symmetry sector with n_{dw} domain walls have the same sizes as the Krylov subspaces in the symmetry sector with $n_{dw}^{\max} - n_{dw}$ domain walls as discussed in Appendix A.

two-dimensional lattice and hexaflake lattice might similarly explain the lack of fragmentation on these lattices in symmetry sectors with a large number of domain walls.

IV. THE AUTOCORRELATION FUNCTION OF LOCAL OBSERVABLES

The autocorrelation function of a local observable is an effective tool for characterizing systems exhibiting HSF [6, 26–28]. For a local operator \mathcal{O} acting within a Hilbert space of dimension \mathcal{D} , the infinite temperature autocor-

relation function at time t is given by

$$\mathcal{A}(t) = \langle \mathcal{O}(t)\mathcal{O}(0) \rangle = \frac{1}{\mathcal{D}} \text{Tr}(e^{iHt}\mathcal{O}e^{-iHt}\mathcal{O}), \quad (5)$$

where $\langle \cdot \rangle = \text{Tr}(\cdot)/\mathcal{D}$ is the infinite temperature expectation value and H is the Hamiltonian operator governing the system. Fragmented models are characterized by parts of the system acting as blockades and thereby restricting the movement within the system. A local observable is, therefore, correlated with itself at later times because the full system is not explored freely. In contrast, thermal systems do not retain local information about their initial state and the autocorrelation functions

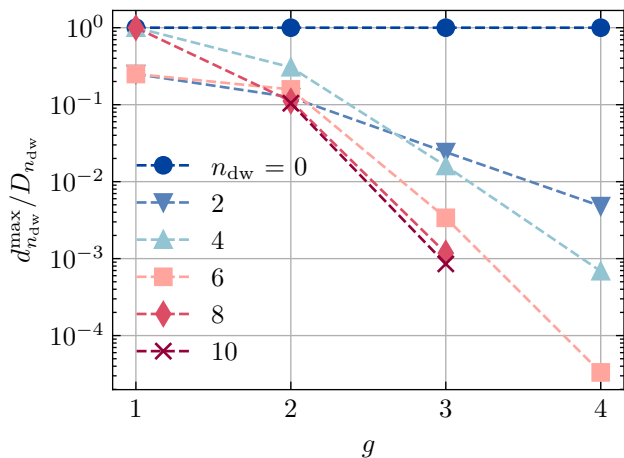


FIG. 4. The ratio between the dimension of the largest Krylov subspace $d_{n_{dw}}^{\max}$ and the dimension of the symmetry sector $D_{n_{dw}}$ as a function of the generation g of the Vicsek fractal lattice. Each graph corresponds to a fixed number of domain walls n_{dw} . The data for generation $g = 1, 2$ is exact while the data for generation $g = 3, 4$ is obtained using Monte Carlo importance sampling as described in Appendix C. The symmetry sector with $n_{dw} = 0$ domain walls is one-dimensional for all generations, and the ratio is unity. For all other considered sectors, the ratio decreases with increasing generation indicating that the system is strongly fragmented.

of local observables vanish. These considerations are formally captured by the Mazur inequality which provides a lower bound on the long-time average of the autocorrelation function [52–54]. The time-averaged autocorrelation function is given by

$$\bar{A}(T) = \frac{1}{T} \int_0^T A(t) dt. \quad (6)$$

Consider a model described by the Hamiltonian H with a set of conserved quantities $\{I_i\}$, i.e., $[I_i, H] = 0$. The Mazur bound is then given by

$$M_{\mathcal{O}} = \sum_{ij} \langle \mathcal{O}^\dagger I_i \rangle [C^{-1}]_{ij} \langle I_j^\dagger \mathcal{O} \rangle, \quad (7)$$

with $C_{ij} = \langle I_i^\dagger I_j \rangle$. The time-averaged autocorrelation function satisfies the Mazur inequality

$$M_{\mathcal{O}} \leq \lim_{T \rightarrow \infty} \bar{A}(T). \quad (8)$$

For a thermal system, the Mazur bound is close to zero, and the infinite time average of the autocorrelation function of generic observables vanishes. On the other hand, the Mazur bound for integrable systems may be significantly different from zero, and the infinite time averaged autocorrelation function does not relax to zero. The autocorrelation function may, therefore, identify nonthermal behavior.

Equation (7) may be simplified by diagonalizing C_{ij} , i.e., choosing $\{I_i\}$ such that $\langle I_i^\dagger I_j \rangle = \delta_{ij}$. Then the

Mazur bound reduces to $M_{\mathcal{O}} = \sum_i |\langle I_i^\dagger \mathcal{O} \rangle|^2$. Equation (8) is trivially satisfied when the set of conserved quantities is taken as the projections onto the energy eigenstates, i.e., $I_i \propto |E_i\rangle\langle E_i|$ where $\{|E_i\rangle\}$ is the set of energy eigenstates. However, the Mazur bound may be finite with only a few terms $|\langle I_i^\dagger \mathcal{O} \rangle|^2$ contributing significantly to $M_{\mathcal{O}}$. In this case, the finite autocorrelation of \mathcal{O} may be attributed directly to the conserved quantities contributing significantly to $M_{\mathcal{O}}$.

For fragmented models, the projection operators onto the Krylov subspaces $\{\mathcal{P}_i\}$ is a set of conserved quantities. The projection operators satisfy $\langle \mathcal{P}_i^\dagger \mathcal{P}_j \rangle = \delta_{ij} d_i / D_{n_{dw}}$ where d_i is the dimension of the i -th Krylov subspace, $D_{n_{dw}}$ is the dimension of the symmetry sector with n_{dw} domain walls, and δ_{ij} is the Kronecker delta. We consider the observable $\tilde{s}_{\mathbf{r}}^z = s_{\mathbf{r}}^z - \langle s_{\mathbf{r}}^z \rangle$ related to the spin-1/2 operator $s_{\mathbf{r}}^z = \sigma_{\mathbf{r}}^z / 2$ at position \mathbf{r} . The Mazur bound is given by

$$M_{\tilde{s}_{\mathbf{r}}^z} = \frac{1}{D_{n_{dw}}} \sum_i \frac{\text{Tr}(\mathcal{P}_i \tilde{s}_{\mathbf{r}}^z)^2}{d_i}. \quad (9)$$

We compute the time-averaged autocorrelation function for the one-dimensional lattice, the second-generation Vicsek fractal lattice, a section of the second-generation hexaflake fractal lattice, the two-dimensional lattice, and the modified two-dimensional lattice. We study two symmetry sectors for the one-dimensional lattice and a single symmetry sector for all other considered lattices. We consider parameter values $\lambda = J = 1$ and $\Delta = 0.1$ in all cases. Figure 5 displays the time-averaged autocorrelation function and the corresponding Mazur bound. In the one-dimensional, scarred model, the time-averaged autocorrelation function converges to a value close to zero. This behavior is expected for a model where the majority of energy eigenstates are thermal. On the four lattices with dimensions larger than one, the Mazur bound is larger than zero, and, consequently, the autocorrelation function converges to a finite value. Hence, the model displays nonthermal behavior on these lattices and the system retains some memory of its initial state. We remark that the Mazur bound is not tight for the considered lattices with dimensions larger than one. However, in appendix D, we show that the Mazur bound becomes tight when the Hamiltonian is perturbed in each Krylov subspace by a random matrix drawn from the Gaussian orthogonal ensemble.

V. CONCLUSION

We generalized a known, one-dimensional, scarred model to higher dimensional lattices. The model displays HSF on the Vicsek fractal lattice of arbitrary dimension, with the Hilbert space shattering into an exponential number of one-dimensional Krylov subspaces. We demonstrated that the largest Krylov subspace constitutes a vanishingly small fraction of the symmetry sector

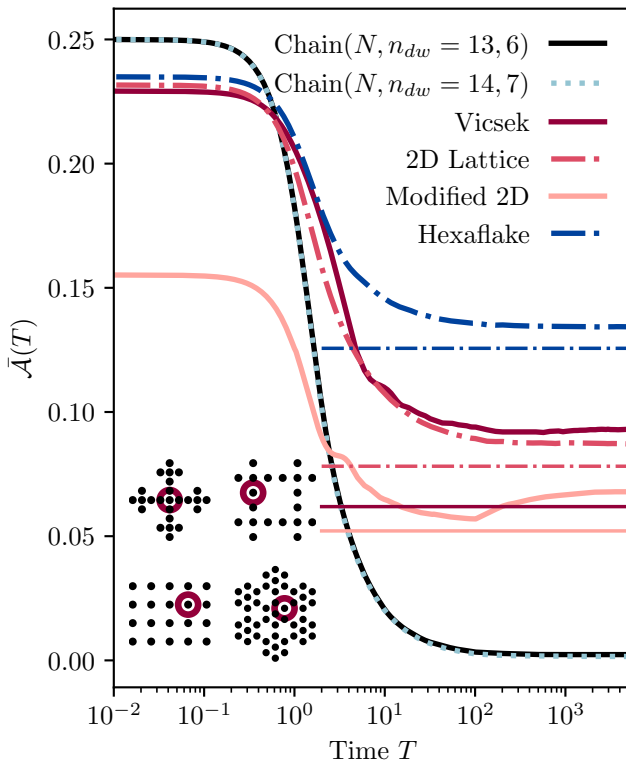


FIG. 5. The time average of the autocorrelation function for the four considered lattices and two symmetry sectors on the one-dimensional lattice of N sites. We consider the symmetry sector $n_{dw} = 6$ ($D_{n_{dw}} = 5472$) for the second-generation Vicsek fractal lattice, $n_{dw} = 14$ ($D_{n_{dw}} = 7680$) for the section of the second-generation hexaflake fractal lattice, $n_{dw} = 14$ ($D_{n_{dw}} = 5323$) for the two-dimensional lattice, and $n_{dw} = 6$ ($D_{n_{dw}} = 3492$) for the modified two-dimensional lattice. We consider the autocorrelation function of the operator $\tilde{s}_r^z = s_r^z - \langle s_r^z \rangle$ for the site \mathbf{r} illustrated in the inset (inside red circle). We find similar results for other sites. In all cases, we consider parameters $\lambda = J = 1$ and $\Delta = 0.1$. The horizontal lines show the Mazur bound obtained from the projection operators onto the Krylov subspaces.

when the number of domain walls is close to zero or close to being maximal. Therefore, the model is strongly fragmented on the Vicsek fractal lattice in these symmetry sectors. Our methods did not allow the analysis of symmetry sectors with the number of domain walls close to half-filling. The model displays features similar to HSF on a section of the second-generation hexaflake fractal lattice, the two-dimensional lattice, and a modified two-dimensional lattice. We studied the time-averaged autocorrelation function of the z -component of a single spin and compared it with the corresponding Mazur bound. We demonstrated that the model displays nonthermal dynamics on all the considered lattices with dimensions larger than one by observing a finite value of the long-time average of the autocorrelation function. We also showed that the Mazur bound becomes tight when the

Hamiltonian is perturbed by a block diagonal random matrix. This work demonstrates that Hilbert space fragmentation may arise solely from the conservation of the number of domain walls in dimensions larger than one and that the nature of the fragmentation depends on the lattice geometry.

ACKNOWLEDGMENTS

This work was supported by Carlsbergfondet under Grant No. CF20-0658 and by Danmarks Frie Forskningsfond under Grant No. 8049-00074B.

Appendix A: Domain wall - domain wall absence symmetry

The Vicsek fractal lattice is bipartite and we denote the two parts by A and B . Let A be the part containing all the dynamically active sites on the boundary of the Vicsek fractal lattice. Recall that we introduced additional spin-down sites along the boundary of the Vicsek fractal lattice in Sec. II to ensure all sites in the original lattice have an even number of nearest neighbors. We note that part A does not contain any of these dynamically inactive sites. We consider the operator

$$T = \bigotimes_{\mathbf{r} \in A} \sigma_{\mathbf{r}}^x, \quad (\text{A1})$$

where $\sigma_{\mathbf{r}}^x$ is the Pauli x -operator acting on site \mathbf{r} . Recall that a domain wall is an edge between two nearest neighbor sites of opposite spin orientations along the z -direction, i.e., $\uparrow\downarrow$ or $\downarrow\uparrow$. We consider a lattice edge to be empty if no domain wall is present and an edge to be occupied if a domain wall is present. The operator T removes all domain walls from occupied edges and inserts domain walls on empty edges. One may show by direct calculation that T commutes with the kinetic part of the Hamiltonian for any generation of the Vicsek fractal lattice $[T, H_\lambda] = 0$. Note, however, that the remaining terms in the Hamiltonian operator do not commute with T . The sizes of the Krylov subspaces in the sector with n_{dw} domain walls are identical to the sizes of the Krylov subspaces in the sector with $n_{dw}^{\max} - n_{dw}$ domain walls where n_{dw}^{\max} is the maximal number of domain walls. To illustrate this point, consider a state $|\psi\rangle$ with n_{dw} domain walls generating the Krylov subspace \mathcal{K} . The corresponding state $|\psi'\rangle = T|\psi\rangle$ obtained by removing domain walls from occupied edges and inserting domain walls on empty edges has $n_{dw}^{\max} - n_{dw}$ domain walls. This state generates a different Krylov subspace \mathcal{K}' . Since T represents a one-to-one correspondence between \mathcal{K} and \mathcal{K}' , the Krylov subspaces have identical dimensions $\dim(\mathcal{K}) = \dim(\mathcal{K}')$. Using this fact, we may, without loss of generality, only consider symmetry sectors with the number of domain walls $n_{dw} \leq n_{dw}^{\max}/2$ on the Vicsek fractal lattice.

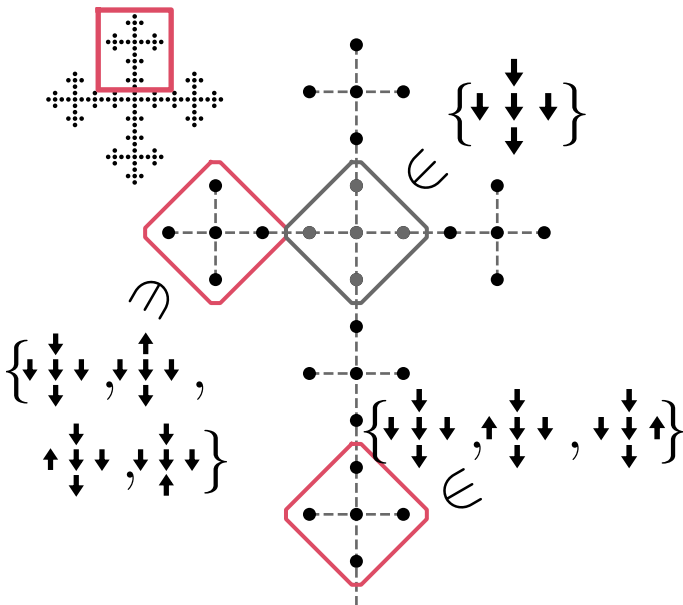


FIG. 6. A part of the Vicsek fractal lattice of generation $g = 3$. We consider the lattice to consist of generation one fractal lattices. Some generation one fractals are nearest neighbors with four other generation one fractals (gray sites). We choose all sites to be spin-down in these generation one fractals. For generation one fractals with two nearest neighbors, the spins are chosen among the three frozen configurations shown in the figure. For generation one fractals with one nearest neighbor, we choose the spins among the four frozen configurations shown in the figure. We construct an exponential number of eigenstates of the Hamiltonian as the tensor product of these frozen configurations on the generation one fractals.

We remark that the hexaflake fractal lattice, the two-dimensional lattice, and the modified two-dimensional lattice are also bipartite and each lattice may be separated into two parts A and B . However, for these lattices, both parts A and B contain some of the dynamically inactive, spin-down sites introduced as padding to the lattices in Sec. II. Consequently, the kinetic part of the Hamiltonian is not invariant under T , and we generally consider all symmetry sectors for these lattices.

Appendix B: Construction of an exponential number of Krylov subspaces on the Vicsek fractal lattice

We prove that the model in Eq. (2) displays Hilbert space fragmentation on the Vicsek fractal lattice of arbitrary generation g by explicitly constructing a set of Krylov subspaces. We focus on one-dimensional Krylov subspaces and demonstrate that the number of such subspaces scales exponentially with the system size.

Consider the Vicsek fractal lattice of generation one.

There exist several “frozen states” where all spins are dynamically inactive. We aim to construct one-dimensional Krylov subspaces for generation $g > 1$ by utilizing the frozen states from generation one. In the following, we consider the Vicsek fractal lattice of generation g to consist of 5^{g-1} generation one fractal lattices. We also consider two generation one fractals to be nearest neighbors if they contain spins that are nearest neighbors. A generation one fractal has one, two, or four other generation one fractals as nearest neighbors as illustrated in Fig. 6. In particular, there are 5^{g-2} generation one fractals with four nearest neighbors. On these generation one fractals, we choose all sites to be spin-down. The remaining $4 \cdot 5^{g-2}$ generation one fractals have either one or two neighbors, and they allow at least three frozen configurations as illustrated in Fig. 6. We construct one-dimensional Krylov subspaces as the tensor product of frozen states on these generation one fractals. There are at least $3^{4 \cdot 5^{g-2}} = (3^{4/25})^N$ such one-dimensional Krylov subspaces where $N = 5^g$ is the total number of sites. The number of Krylov subspaces, hence, grows exponentially with system size and the model from Eq. (2) on the Vicsek fractal lattice displays Hilbert space fragmentation.

Appendix C: Estimation of sector sizes and Krylov subspace dimensions

Let $|s_1 \dots s_N\rangle$ with $s_i \in \{-1/2, 1/2\}$ be a simultaneous eigenket of the Pauli z -operators $\{\sigma_r^z\}$. We consider the indicator function $\mathbb{1}_{n_{\text{dw}}}$ which signals whether $|s_1 \dots s_N\rangle$ belongs to the symmetry sector with n_{dw} domain walls

$$\mathbb{1}_{n_{\text{dw}}}(|s_1 \dots s_N\rangle) = \begin{cases} 1, & \text{if } |s_1 \dots s_N\rangle \text{ has } n_{\text{dw}} \\ & \text{domain walls,} \\ 0, & \text{otherwise.} \end{cases} \quad (\text{C1})$$

The dimension of the symmetry sector with n_{dw} domain walls is given by

$$D_{n_{\text{dw}}} = \sum_{s_1, \dots, s_N} \mathbb{1}_{n_{\text{dw}}}(|s_1 \dots s_N\rangle) \quad (\text{C2})$$

where the sum covers all 2^N possible configurations of the N spins. Equation (C2) is impractical to evaluate numerically for large system sizes since the sum contains an exponential number of terms. We circumvent this problem by employing Monte Carlo importance sampling. We randomly draw $N_{\text{MC}} \ll 2^N$ product states $\{|\psi_i\rangle\}_{i=1}^{N_{\text{MC}}}$ that are simultaneous eigenkets of the Pauli z -operators. Each product state is drawn independently from the probability distribution P_p parameterized by $p \in [0, 1]$

$$P_p(|s_1 \dots s_N\rangle) = \prod_{i=1}^N p^{1/2+s_i} (1-p)^{1/2-s_i}. \quad (\text{C3})$$

In other words, we draw each spin independently with probability p of being spin-up and probability $1-p$ of

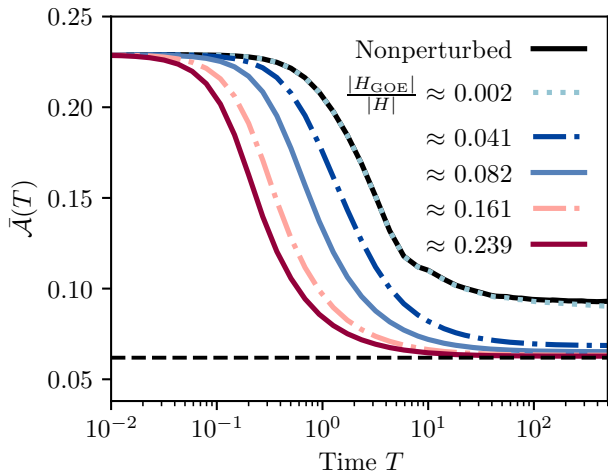


FIG. 7. The time-averaged autocorrelation function on the Vicsek fractal lattice for the perturbed Hamiltonian from Eq. (D1). The size of the perturbation is characterized by the ratio between the Frobenius norm of the perturbation matrix $|H_{\text{GOE}}|$ to that of the nonperturbed Hamiltonian $|H|$. The dashed line displays the Mazur bound obtained from the projection operators onto the Krylov subspaces.

being spin-down. The sector size is estimated by

$$\tilde{D}_{n_{\text{dw}}} = \frac{1}{N_{\text{MC}}} \sum_{i=1}^{N_{\text{MC}}} \frac{\mathbb{1}_{n_{\text{dw}}}(|\psi_i\rangle)}{P_p(|\psi_i\rangle)}. \quad (\text{C4})$$

and the estimate of the variance of $\tilde{D}_{n_{\text{dw}}}$ is given by

$$\sigma^2 = \frac{1}{N_{\text{MC}}(N_{\text{MC}} - 1)} \sum_{i=1}^{N_{\text{MC}}} \left[\frac{\mathbb{1}_{n_{\text{dw}}}(|\psi_i\rangle)}{P_p(|\psi_i\rangle)} - \tilde{D}_{n_{\text{dw}}} \right]^2. \quad (\text{C5})$$

For each generation g and symmetry sector n_{dw} , we sample from the probability distribution P_p which minimizes the variance, i.e., we perform a grid search and choose the p that yields the smallest variance.

After computing $\tilde{D}_{n_{\text{dw}}}$, we estimate the dimension of the largest Krylov subspace in this sector. The largest Krylov subspace is determined from an exhaustive search of the full sector. We randomly draw a product state with n_{dw} domain walls. We determine in which Krylov subspace the state resides and record the dimension of this subspace. We repeat this procedure until $\tilde{D}_{n_{\text{dw}}} - \tilde{d}_{n_{\text{dw}}}^{\text{max}}$ different product states have been found where $\tilde{d}_{n_{\text{dw}}}^{\text{max}}$ is the size of the largest Krylov subspace found so far. The dimension of the largest Krylov subspace is then estimated by $\tilde{d}_{n_{\text{dw}}}^{\text{max}}$ after the search finishes.

Appendix D: Perturbing the Hamiltonian with a random matrix

In Sec. IV, we observe that the time-averaged autocorrelation function does not converge to the Mazur bound obtained from the projection operators onto the Krylov subspaces. In this appendix, we demonstrate that the Mazur bound becomes tight when the Hamiltonian operator is perturbed. We perturb the Hamiltonian operator by a block diagonal matrix whose blocks are drawn from the Gaussian orthogonal ensemble (GOE). The GOE consists of symmetric matrices where the entries follow the normal distribution $N(\mu, \sigma^2)$. The diagonal entries have zero mean and variance $\sigma^2 = 2$, i.e., $G_{ii} \sim N(0, 2)$, while the off-diagonal entries have zero mean and unit variance, i.e., $G_{ij} \sim N(0, 1)$ for $i \neq j$. The entries are independent up to the symmetry requirement, i.e., $G_{ij} = G_{ji}$ [55]. The block diagonal structure is chosen to overlap with that of the kinetic term of the Hamiltonian to conserve the HSF. The Hamiltonian is given by

$$H' = H + H_{\text{GOE}} = H_\lambda + H_z + H_{zz} + H_{\text{GOE}}, \quad (\text{D1})$$

where the terms H_λ , H_z and H_{zz} are defined in Eq. (3) and $H_{\text{GOE}} = \epsilon G$, where G is a block diagonal matrix of GOE matrices and $\epsilon \in \mathbb{R}$ is a strength parameter. We characterize the strength of the perturbation by the ratio of the Frobenius norms. Figure 7 shows that the time-averaged autocorrelation function for the chosen spin operator converges to the Mazur bound when the Hamiltonian is perturbed.

-
- [1] M. Srednicki, Chaos and quantum thermalization, Phys. Rev. E **50**, 888 (1994).
 - [2] J. M. Deutsch, Quantum statistical mechanics in a closed system, Phys. Rev. A **43**, 2046 (1991).
 - [3] M. Rigol, V. Dunjko, and M. Olshanii, Thermalization and its mechanism for generic isolated quantum systems, Nature **452**, 854 (2008).
 - [4] A. P. Luca D'Alessio, Yariv Kafri and M. Rigol, From quantum chaos and eigenstate thermalization to statistical mechanics and thermodynamics, Advances in Physics **65**, 239 (2016).
 - [5] M. Serbyn, D. A. Abanin, and Z. Papić, Quantum many-body scars and weak breaking of ergodicity, Nature Physics **17**, 675 (2021).
 - [6] S. Moudgalya, B. A. Bernevig, and N. Regnault, Quantum many-body scars and Hilbert space fragmentation: a review of exact results, Reports on Progress in Physics **85**, 086501 (2022).
 - [7] A. Chandran, T. Iadecola, V. Khemani, and R. Moessner, Quantum many-body scars: A quasiparticle perspective, Annual Review of Condensed Matter Physics **14**, 443 (2023).
 - [8] D. P. Arovas, Two exact excited states for the $S = 1$ AKLT chain, Physics Letters A **137**, 431 (1989).
 - [9] S. Moudgalya, S. Rachel, B. A. Bernevig, and N. Regnault, Exact excited states of nonintegrable models,

- Phys. Rev. B **98**, 235155 (2018).
- [10] S. Moudgalya, N. Regnault, and B. A. Bernevig, Entanglement of exact excited states of Affleck-Kennedy-Lieb-Tasaki models: Exact results, many-body scars, and violation of the strong eigenstate thermalization hypothesis, Phys. Rev. B **98**, 235156 (2018).
- [11] H. Bernien, S. Schwartz, A. Keesling, H. Levine, A. Omran, H. Pichler, S. Choi, A. S. Zibrov, M. Endres, M. Greiner, V. Vuletić, and M. D. Lukin, Probing many-body dynamics on a 51-atom quantum simulator, Nature **551**, 579 (2017).
- [12] T. Iadecola, M. Schechter, and S. Xu, Quantum many-body scars from magnon condensation, Phys. Rev. B **100**, 184312 (2019).
- [13] M. Schechter and T. Iadecola, Weak ergodicity breaking and quantum many-body scars in spin-1 XY magnets, Phys. Rev. Lett. **123**, 147201 (2019).
- [14] N. Shibata, N. Yoshioka, and H. Katsura, Onsager's scars in disordered spin chains, Phys. Rev. Lett. **124**, 180604 (2020).
- [15] D. K. Mark and O. I. Motrunich, η -pairing states as true scars in an extended Hubbard model, Phys. Rev. B **102**, 075132 (2020).
- [16] S. Moudgalya, E. O'Brien, B. A. Bernevig, P. Fendley, and N. Regnault, Large classes of quantum scarred Hamiltonians from matrix product states, Phys. Rev. B **102**, 085120 (2020).
- [17] T. Iadecola and M. Schechter, Quantum many-body scar states with emergent kinetic constraints and finite-entanglement revivals, Physical Review B **101**, 024306 (2020).
- [18] E. Chertkov and B. K. Clark, Motif magnetism and quantum many-body scars, Phys. Rev. B **104**, 104410 (2021).
- [19] J. Wildeboer, A. Seidel, N. S. Srivatsa, A. E. B. Nielsen, and O. Erten, Topological quantum many-body scars in quantum dimer models on the kagome lattice, Phys. Rev. B **104**, L121103 (2021).
- [20] D. Bluvstein, A. Omran, H. Levine, A. Keesling, G. Semeghini, S. Ebadi, T. T. Wang, A. A. Michailidis, N. Maskara, W. W. Ho, S. Choi, M. Serbyn, M. Greiner, V. Vuletić, and M. D. Lukin, Controlling quantum many-body dynamics in driven Rydberg atom arrays, Science **371**, 1355 (2021).
- [21] I.-C. Chen, B. Burdick, Y. Yao, P. P. Orth, and T. Iadecola, Error-mitigated simulation of quantum many-body scars on quantum computers with pulse-level control, Phys. Rev. Res. **4**, 043027 (2022).
- [22] P. Zhang, H. Dong, Y. Gao, L. Zhao, J. Hao, J.-Y. Desaulles, Q. Guo, J. Chen, J. Deng, B. Liu, W. Ren, Y. Yao, X. Zhang, S. Xu, K. Wang, F. Jin, X. Zhu, B. Zhang, H. Li, C. Song, Z. Wang, F. Liu, Z. Papić, L. Ying, H. Wang, and Y.-C. Lai, Many-body Hilbert space scarring on a superconducting processor, Nature Physics **19**, 120 (2023).
- [23] G.-X. Su, H. Sun, A. Hudomal, J.-Y. Desaulles, Z.-Y. Zhou, B. Yang, J. C. Halimeh, Z.-S. Yuan, Z. Papić, and J.-W. Pan, Observation of many-body scarring in a Bose-Hubbard quantum simulator, Phys. Rev. Res. **5**, 023010 (2023).
- [24] H. Zhou, H. Gao, N. T. Leitaó, O. Makarova, I. Cong, A. M. Douglas, L. S. Martin, and M. D. Lukin, Robust Hamiltonian engineering for interacting qudit systems (2023), arXiv:2305.09757 [quant-ph].
- [25] E. J. Gustafson, A. C. Y. Li, A. Khan, J. Kim, D. M. Kurkcuoglu, M. S. Alam, P. P. Orth, A. Rahmani, and T. Iadecola, Preparing quantum many-body scar states on quantum computers, Quantum **7**, 1171 (2023).
- [26] T. Rakovszky, P. Sala, R. Verresen, M. Knap, and F. Pollmann, Statistical localization: From strong fragmentation to strong edge modes, Phys. Rev. B **101**, 125126 (2020).
- [27] S. Moudgalya and O. I. Motrunich, Hilbert space fragmentation and commutant algebras, Phys. Rev. X **12**, 011050 (2022).
- [28] P. Sala, T. Rakovszky, R. Verresen, M. Knap, and F. Pollmann, Ergodicity breaking arising from Hilbert space fragmentation in dipole-conserving Hamiltonians, Phys. Rev. X **10**, 011047 (2020).
- [29] S. Moudgalya, A. Prem, R. Nandkishore, N. Regnault, and B. A. Bernevig, Thermalization and its absence within Krylov subspaces of a constrained Hamiltonian, in *Memorial Volume for Shoucheng Zhang* (WORLD SCIENTIFIC, 2021) pp. 147–209.
- [30] G. De Tomasi, D. Hetterich, P. Sala, and F. Pollmann, Dynamics of strongly interacting systems: From Fock-space fragmentation to many-body localization, Phys. Rev. B **100**, 214313 (2019).
- [31] L. Herviou, J. H. Bardarson, and N. Regnault, Many-body localization in a fragmented Hilbert space, Phys. Rev. B **103**, 134207 (2021).
- [32] S. Pai, M. Pretko, and R. M. Nandkishore, Localization in fractonic random circuits, Phys. Rev. X **9**, 021003 (2019).
- [33] A. Morningstar, V. Khemani, and D. A. Huse, Kinetically constrained freezing transition in a dipole-conserving system, Phys. Rev. B **101**, 214205 (2020).
- [34] V. Khemani, M. Hermele, and R. Nandkishore, Localization from Hilbert space shattering: From theory to physical realizations, Phys. Rev. B **101**, 174204 (2020).
- [35] Z.-C. Yang, F. Liu, A. V. Gorshkov, and T. Iadecola, Hilbert-space fragmentation from strict confinement, Phys. Rev. Lett. **124**, 207602 (2020).
- [36] K. Lee, A. Pal, and H. J. Changlani, Frustration-induced emergent Hilbert space fragmentation, Phys. Rev. B **103**, 235133 (2021).
- [37] D. Hahn, P. A. McClarty, and D. J. Luitz, Information dynamics in a model with Hilbert space fragmentation, SciPost Phys. **11**, 074 (2021).
- [38] C. M. Langlett and S. Xu, Hilbert space fragmentation and exact scars of generalized Fredkin spin chains, Phys. Rev. B **103**, L220304 (2021).
- [39] B. Mukherjee, Z. Cai, and W. V. Liu, Constraint-induced breaking and restoration of ergodicity in spin-1 PXP models, Phys. Rev. Res. **3**, 033201 (2021).
- [40] B. Mukherjee, D. Banerjee, K. Sengupta, and A. Sen, Minimal model for Hilbert space fragmentation with local constraints, Phys. Rev. B **104**, 155117 (2021).
- [41] W.-H. Li, X. Deng, and L. Santos, Hilbert space shattering and disorder-free localization in polar lattice gases, Phys. Rev. Lett. **127**, 260601 (2021).
- [42] A. Bastianello, U. Borla, and S. Moroz, Fragmentation and emergent integrable transport in the weakly tilted Ising chain, Phys. Rev. Lett. **128**, 196601 (2022).
- [43] J. Richter and A. Pal, Anomalous hydrodynamics in a class of scarred frustration-free Hamiltonians, Phys. Rev. Res. **4**, L012003 (2022).

- [44] P. Brighi, M. Ljubotina, and M. Serbyn, Hilbert space fragmentation and slow dynamics in particle-conserving quantum east models, *SciPost Phys.* **15**, 093 (2023).
- [45] S. R. Taylor, M. Schulz, F. Pollmann, and R. Moessner, Experimental probes of Stark many-body localization, *Phys. Rev. B* **102**, 054206 (2020).
- [46] E. V. H. Doggen, I. V. Gornyi, and D. G. Polyakov, Stark many-body localization: Evidence for Hilbert-space shattering, *Phys. Rev. B* **103**, L100202 (2021).
- [47] S. Scherg, T. Kohlert, P. Sala, F. Pollmann, B. Hebbe Madhusudhana, I. Bloch, and M. Aidelsburger, Observing non-ergodicity due to kinetic constraints in tilted Fermi-Hubbard chains, *Nature Communications* **12**, 4490 (2021).
- [48] T. Kohlert, S. Scherg, P. Sala, F. Pollmann, B. H. Madhusudhana, I. Bloch, and M. Aidelsburger, Experimental realization of fragmented models in tilted Fermi-Hubbard chains (2021), arXiv:2106.15586 [cond-mat.quant-gas].
- [49] L. Caha and D. Nagaj, The pair-flip model: a very entangled translationally invariant spin chain (2018), arXiv:1805.07168 [quant-ph].
- [50] A. Khudorozhkov, A. Tiwari, C. Chamon, and T. Neupert, Hilbert space fragmentation in a 2D quantum spin system with subsystem symmetries, *SciPost Phys.* **13**, 098 (2022).
- [51] A. Chattopadhyay, B. Mukherjee, K. Sengupta, and A. Sen, Strong Hilbert space fragmentation via emergent quantum drums in two dimensions, *SciPost Phys.* **14**, 146 (2023).
- [52] P. Mazur, Non-ergodicity of phase functions in certain systems, *Physica* **43**, 533 (1969).
- [53] M. Suzuki, Ergodicity, constants of motion, and bounds for susceptibilities, *Physica* **51**, 277 (1971).
- [54] A. Dhar, A. Kundu, and K. Saito, Revisiting the Mazur bound and the Suzuki equality, *Chaos, Solitons & Fractals* **144**, 110618 (2021).
- [55] G. W. Anderson, A. Guionnet, and O. Zeitouni, *An Introduction to Random Matrices*, Cambridge Studies in Advanced Mathematics (Cambridge University Press, 2009).